Acta Oceanol. Sin., 2022, Vol. 41, No. 7, P. 54–64
https://doi.org/10.1007/s13131-021-1952-6
http://www.aosocean.com
E-mail: ocean2@hyxb.org.cn

Variability of the deep South China Sea circulation derived from HYCOM reanalysis data

Yaohua Zhu[1, 2, 3], Guojiao Cao[4], Yonggang Wang[1, 2, 3], Shujiang Li[1, 2, 3], Tengfei Xu[1, 2, 3], Dingqi Wang[1, 5], Fei Teng[1, 2, 3], Zexun Wei[1, 2, 3*]

[1] First Institute of Oceanography, and Key Laboratory of Marine Science and Numerical Modeling, Ministry of Natural Resources, Qingdao 266061, China

[2] Laboratory for Regional Oceanography and Numerical Modeling, Pilot National Laboratory for Marine Science and Technology (Qingdao), Qingdao 266237, China

[3] Shandong Key Laboratory of Marine Science and Numerical Modeling, Qingdao 266061, China

[4] Navigation College, Jiangsu Maritime Institute, Nanjing 211100, China

[5] College of Oceanic and Atmospheric Sciences, Ocean University of China, Qingdao 266100, China

Received 22 July 2021; accepted 26 August 2021

Abstract

This study aims to investigate variability of the deep South China Sea (SCS) circulation using the Hybrid Coordinate Ocean Model (HYCOM) global reanalysis product. The results reveal that annual cycle is a dominant component in the deep SCS circulation. Meanwhile, the boundary circulation strength is the weakest in January and peaks between June and September. The eastern and southern boundary currents strengthen/weaken one to three months earlier than that in the western and northern boundaries. Vector Empirical Orthogonal Functions (VEOF) analysis results reveal that semiannual and intraseasonal fluctuations are significant components, of which the spatial patterns are mainly confined in the northern and western boundary areas as well as the southwestern sub-basin. Wavelet analysis results show the strength of significant fluctuation varies year to year. Trend analysis results indicate a decadal weakening in the deep SCS circulation. An anomalous anticyclonic circulation, 50–70 km apart from the slope break, tends to weaken the cyclonic boundary circulation in the western and northern boundaries as well as the southwestern sub-basin. This trend is similar to the observed decadal weakening in the North Atlantic deep circulation. Thus, the findings of this study reveal that the variation of the deep SCS circulation has a remarkable response to the climate change. The mechanisms responsible for the variation are worth pursuing if more observations are available.

Key words: South China Sea, variability of deep circulation, HYCOM data, VEOF analysis, wavelet analysis

Citation: Zhu Yaohua, Cao Guojiao, Wang Yonggang, Li Shujiang, Xu Tengfei, Wang Dingqi, Teng Fei, Wei Zexun. 2022. Variability of the deep South China Sea circulation derived from HYCOM reanalysis data. Acta Oceanologica Sinica, 41(7): 54–64, doi: 10.1007/s13131-021-1952-6

1 Introduction

The South China Sea (SCS) is the largest marginal sea in the tropical western Pacific. Below 200 m depth, the deep SCS basin is semi-enclosed (Wyrtki, 1961). It connects with the western Pacific through its sole deepwater renewal channel, the Luzon Strait. Oriented northeast–southwest and confined into a diamond-shaped region, the deep SCS basin can be divided into the northeastern (NE), northwestern (NW), southwestern (SW), southeastern (SE) and central sub-basins. In the middle, the Xisha Islands, Zhongsha Islands and Huangyan Island (i.e., Scarborough Shoal) combine an east-westward chain of islands and seamounts across the central basin, separating the central basin into the northern and southern central sub-basins (Fig. 1). The circulation pattern in the two central sub-basins may differ as deep water exchange is partially impeded by this island chain (Zhu et al., 2019).

The deep circulation in the SCS is driven by the Luzon Strait deepwater overflow below the depth of 1 500 m from the western Pacific, which is forced by a persistent pressure gradient across the Luzon Strait (Qu et al., 2006; Li and Qu, 2006; Zhao et al., 2014; Zhang et al., 2015). The time-mean circulation in the deep SCS basin is known as cyclonic inferred from observations (Wang, 1986; Qu et al., 2006; Li and Qu, 2006; Shao et al., 2007; Wang et al., 2011; Zhu et al., 2017a) and simulated by numerical models (Chao et al., 1996; Yuan, 2002; Lan et al., 2013; Xie et al., 2013; Xiao et al., 2013; Wang and Zhao, 2013; Shu et al., 2014; Xu and Oey, 2014; Gan et al., 2016a, b).

Nevertheless, being the difficulty in study of the deep SCS circulation, its variability is still not clear due to lack of long-term and large-scale observations. Hitherto, a few pioneering works were engaged in the variability of deep circulation by means of seasonal mean climatology of current velocities. Among them, the numerical simulation of Lan et al. (2015) and Gan et al. (2016a, b) suggested a stronger circulation in summer than that in winter. Zheng et al. (2021) also found the southwestward boundary currents are strong in summer and autumn but insig-

Foundation item: The National Key Research and Development Program of China under contract No. 2019YFC1408400; the National Natural Science Foundation of China under contract Nos 41876029 and 41821004.
*Corresponding author, E-mail: weizx@fio.org.cn

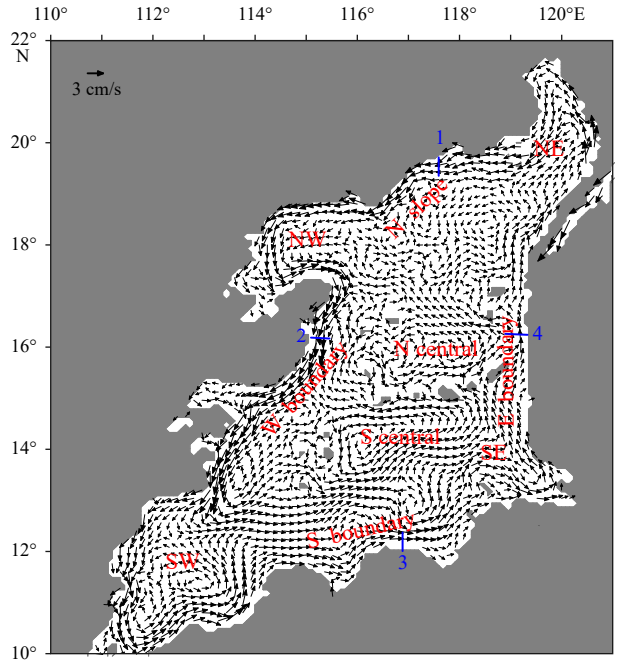

Fig. 1. Time-mean current velocity field at 3 000 m depth. The grey shading indicates water depths shallower than 3 000 m. Abbreviations NE, NW, SW, and SE denote the northeastern, northwestern, southwestern, and southeastern sub-basins, respectively. N central and S central indicate the northern and southern central sub-basins, respectively. Blue lines stand for transects through which monthly mean climatology of the deep boundary circulation is estimated.

nificant in winter and spring to the east and northeast of the Zhongsha Islands during their mooring observation between July 2016 and April 2019. On the other hand, being the driving force of the deep SCS circulation, the Luzon Strait deepwater overflow is of a maximum transport in late fall and minimum in spring as observed by Zhou et al. (2014), simulated by Zhao et al. (2014), and estimated by Zhu et al. (2017b). The inconclusive seasonality motivates us to learn more details about the variability of the deep circulation in the SCS.

Besides the seasonality, other time-scale variations also exist in the deep ocean. For instance, the deep current at the western boundary of the northern Philippine Basin is modulated by intraseasonal variability with period of 30–80 d (Zhou et al., 2018). Significant intraseasonal variations were also identified in velocity along the Luzon Strait (Zhou et al., 2014). The dominant time scales of fluctuation range between 20 d and 60 d in the Bashi Channel and Luzon Trough, and around 100 d in the Luzon Trough. In the western boundary area, intraseasonal fluctuations in 90 d were detected in the boundary current southeast of the Zhongsha Islands (Zhou et al., 2017). As the observations are still extremely sparse compared to the vast deep basin covering the area of 1×10^6 km^2 below 2 000 m, one might wonder: Do these intraseasonal fluctuations observed at specific locations exist ubiquitously in the deep SCS basin? If other variations do exist, what are the typical pattern and dominant variation in the basin scale circulation? Being related to both local and global climate, the variability in the deep SCS circulation is an important issue to be addressed although observations are inadequate at this stage.

In this study, we attempt to identify the variability in the deep SCS circulation based on a validated reanalysis product by presenting the monthly mean climatology, analyzing the decadal change, and decomposing series of velocity vector fields. Time-domain Vector Empirical Orthogonal Functions (VEOF) analysis is used in this study. This method has been proved successful in identifying variation in wind stress and upper layer circulation in the SCS. For example, Wu et al. (1998) implemented this method to the velocity field at 50 m depth in the SCS from their 4-year numerical simulation sampled every 10 d. Their analysis revealed a symmetric seasonally reversing southern gyre in the first VEOF mode, and a northern gyre responsible for asymmetric seasonal and interannual variations in the second VEOF mode. Fang et al. (2006) applied VEOF analysis to evaluate interannual variability of surface wind over the SCS, and found that the surface wind shows a significant correlation with the ENSO variability. In the meantime, Wang et al. (2006) adopted VEOF analysis to a 23-year monthly current velocity field simulated from a variable-grid global ocean circulation model. Their results suggested that the upper layer circulation in the SCS is closely correlated with the ENSO variability, but the circulation at 510 m depth shows a decreasing correlation with the ENSO Index. With initial pictures of monthly mean climatology, decadal trend, spatial patterns and temporal variations in the deep SCS circulation, the present work may offer some beneficial enlightenment to the study on the variability of the deep SCS circulation. The rest of the paper is organized as follows. In Section 2, we briefly introduce the data and fidelity. Section 3 describes the annual cycle and trend of the deep circulation, and findings from the VEOF analysis, followed by a summary in Section 4.

2 Data and validation

As the Luzon Strait deepwater overflow is the crucial force to drive the deep SCS circulation, a model of relatively high-resolution is essential to reasonably simulate the overflow in the Luzon Strait. Response of the deep circulation in the SCS to horizontal resolution was examined by Wang and Zhao (2013). They found that a horizontal resolution of (1/12)° can sufficiently reflect the complex topography in the Bashi Channel and Luzon Trough, whereas a (1/6)° grid is too coarse to reproduce the Luzon Strait deepwater overflow. For this reason, a 22-year (1994–2015) global Hybrid Coordinate Ocean Model (HYCOM) reanalysis with the Navy Coupled Ocean Data Assimilation is used. The HYCOM production is the global ocean forecasting system (GOFS) version 3.1 with a horizontal resolution of 0.08°×0.08° between 40°N and 40°S run by the Naval Research Laboratory of U.S. Navy (http://hycom.org/dataserver/glb-analysis). Compared to its previous version (i.e., GOFS version 3.0), the GOFS3.1 is of several significant improvements relevant to our present study, including: (1) 17 terms in the equation of state instead of 7 terms in the GOFS3.0; (2) calculating ocean turbidity based on monthly chlorophyll climatology instead of photosynthetically available radiation; (3) initialized from the GDEM4.0 climatology rather than from the Polar Science Center Hydrography in the GOFS3.0; (4) using relatively weak SSS relaxation. Recently, we have carefully validated the HYCOM GOFS3.1 reanalysis production with long-term observations in the deep western boundary current (DWBC) and Karimata Strait. In the deep layer, the time-mean alongshore velocity from both mooring observations and reanalysis production manifests a similar bottom-intensified southwestward DWBC core leaning on the slope break. In the core region of the DWBC southeast of the Zhongsha Islands, the mean boundary current of 3 cm/s and associated standard deviation of 4.5 cm/s from the HYCOM reanalysis are fairly congruent with the mooring observations in Zhou et al. (2017). The monthly climatology of the DWBC from both observations and reanalysis

production further shows a robust southwestward core from April to September and a weak DWBC from October to March. The DWBC east and northeast of the Zhongsha Islands from the HYCOM reanalysis is of a southwestward mean velocity of 2.5 cm/s with its maximum monthly climatology occurring in August, showing a good agreement with the 3-year mooring observations in Zheng et al. (2021). On the other hand, variability of transports in the major straits is an important way to validate the model simulation. The HYCOM reanalysis also captures a highly consistent variability with the 10-year observations in the Karimata Strait transport (Xu et al., 2021). The latter is the longest available observational transport among all the straits connecting the SCS and adjacent seas. The correlation coefficient between these two transport time series is as high as 0.98. As the HYCOM GOFS3.1 reanalysis has been successfully validated in the depth, strength and monthly climatology in the DWBC and transport variability in the Karimata Strait, it is expected to provide a reasonable performance in simulating the deep SCS circulation. Results are presented in the following section.

3 Results

3.1 *Mean characteristics of the deep SCS circulation*

The horizontal circulation at 3 000 m depth and vertically-averaged circulation between 2 500 m and 4 000 m (see Appendix) manifest a similarly cyclonic pattern around the SCS continental slope, indicative of a basically homogenous circulation in vertical. This homogeneity of the cyclonic circulation was attributed to the enhanced diapycnal mixing in the deep SCS basin (Tian et al., 2009). Wang et al. (2011) computed geostrophic current with thermal wind relation using the GDEM3.0, and also revealed a rather homogeneous cyclonic circulation from 2 400 m to the bottom in the SCS. Based on numerical modeling and absolute geostrophic current, respectively, Gan et al. (2016a) and Zhu et al. (2017a) obtained a positive domain-averaged vorticity homogeneously below 2 000 m. For this reason, we choose the horizontal circulation at 3 000 m depth as a proxy of the deep circulation in the SCS, which avoids a fictitious weakening and widening boundary currents from vertical averaging. Another reason we choose the circulation at 3 000 m is this depth is away from the sill depth of the Luzon Strait and abyssal seabed, where possible vertical velocity shear or bottom intensification may occur.

The 22-year mean circulation at 3 000 m depth is characterized by a clearly cyclonic circulation along the SCS continental slope, starting with a northeastward flow of the Luzon Strait deepwater overflow, then a southwestward flow along the northern slope and western boundary, and then eastward flow along the southern boundary and northward flow along the eastern boundary (Fig. 1). The boundary currents are significantly strong along the northern slope, western boundary and SW sub-basin and reach approximately 3 cm/s, congruent with the long-term mooring observations in Zhou et al. (2017) and Zheng et al. (2021). This basin-scale cyclonic circulation is consistent with previous studies based on geostrophic current and numerical modeling (Wang et al., 2011; Lan et al., 2013, 2015; Gan et al., 2016a, b; Zhu et al., 2017a). Confined by topography and boundary currents, cyclonic eddy is also evident in the NE, NW, SW, and SE sub-basins. Two eddies in the northern and southern central sub-basins are separated by the island chain across the central basin, showing a good agreement with the absolute geostrophic currents derived from GDEM3.0 (Zhu et al., 2017a). Standard deviations (STDs) of eastward component (u) reveal an energetic variation along the northern and southern slopes, while the STDs of the northward component (v) of current velocity show an energetic variation in the DWBC core area, SW sub-basin and eastern boundary (Figs 2a, b). The maximum STDs of u and v components exceed 3 cm/s, which produce a velocity variation as large as 4–5 cm/s, that is, twice of the mean current velocity as observed by Zhou et al. (2017).

3.2 *Annual variability of the deep SCS circulation*

The circulation in the SCS is experienced the influence of the

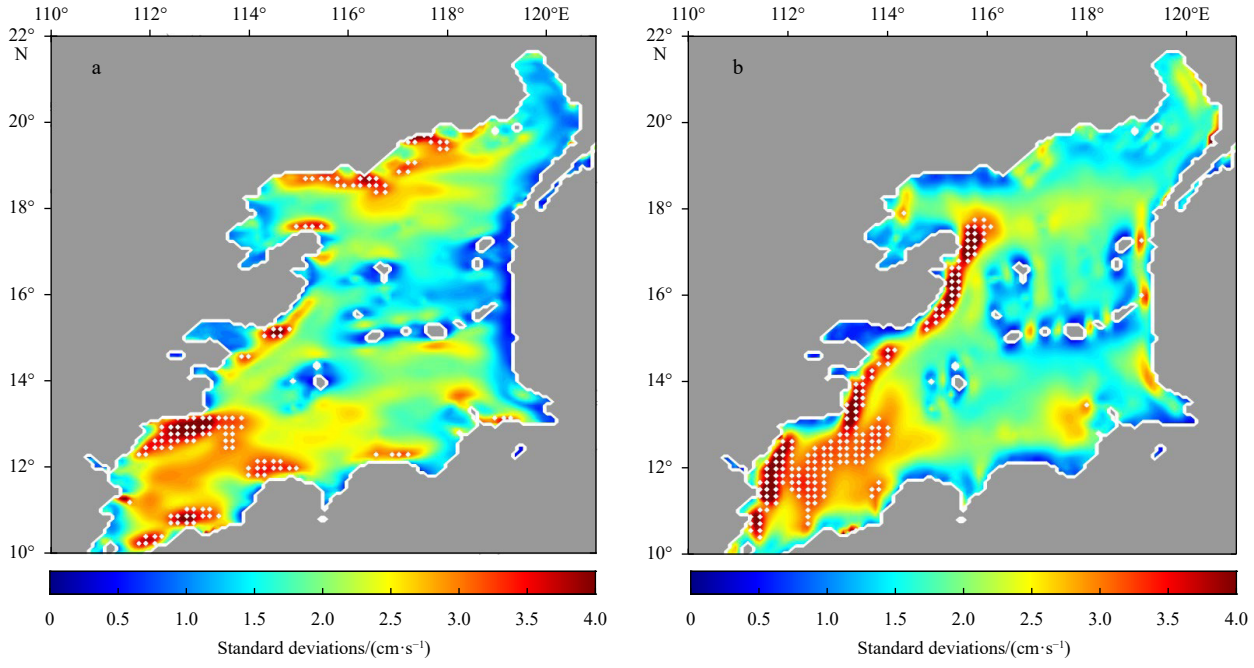

Fig. 2. Standard deviations (STDs) of u (a), and v (b) components at 3 000 m, respectively. Stippled area denotes STDs greater than 3 cm/s.

East Asian monsoon, which reverses its direction from northeasterly in winter to southwesterly in summer. Direct VEOF analysis of the current velocity fields at 3 000 m shows a dominant annual variation. The spectrum analysis of the associated time coefficient functions (or principal component, PC) reveals dominant fluctuation with period of 357 d (figures not shown). To discuss the annual variation of the deep circulation, we present monthly mean climatology of the deep circulation in this section. Accordingly, the annual cycle will be removed for VEOF analysis in the follow section.

January is a month of the weakest circulation in the deep SCS basin. Boundary currents along the northern slope and western boundary and eddies in the central sub-basins are weak (Fig. 3b). Remarkable phenomena are the cyclonic eddy in the NW sub-basin and dipole eddies in the SW sub-basin, i.e., an anticyclonic eddy in the west and a cyclonic eddy in the east. In February, the anticyclonic eddy disappears in the SW sub-basin (Fig. 3c). Boundary currents grow gradually from March to June (Figs 3d–f and 4a) and reach a prosperous phase in July and August. Cyclonic eddies form in both northern and southern central sub-basins. In particular, the one in the southern sub-basin merges the cyclonic eddy in the SE sub-basin and currents along the southern boundary into a large cyclonic gyre (Figs 4b, c). The eastern boundary currents and cyclonic eddy in the SE sub-basin start to weaken in September (Fig. 4d). In the following month, the currents along the southern boundary and cyclonic eddy in the SW sub-basin weaken sequentially, when the currents along the northern slope and western boundary remain robust (Fig. 4e). The eddy in the SW, SE, and central sub-basins weakens remarkably in November (Fig. 4f). In December, the currents along the northern slope and western boundary further decrease, while the interior circulation is in its recession phase and the eddy in the SW sub-basin turns anticyclonic (Fig. 3a).

As seen from the monthly mean climatology of the deep SCS circulation, the boundary currents grow and weaken in different phase around the deep SCS basin. To identify the phase of the boundary currents, we set 4 transects to estimate the climatological volume flux of the boundary currents, including two meridional transects across the northern slope and southern boundary and two zonal transects across the eastern and western boundaries (marked in blue lines in Fig. 1). The normalized flux attains its minimum in the eastern boundary in November, one month earlier than that in the southern boundary and two months earlier than those in the western boundary and northern slope (Fig. 5). All the boundary currents strengthen in the next few months. The currents along the eastern boundary peak in May, two months earlier than those along the southern and western boundaries and three months earlier than those along the northern slope. The boundary currents along the eastern and southern boundaries weaken quickly after July, while those along the northern slope and western boundary remain their robust status for three more months and weaken after October. In other words, the currents grow and weaken earlier along the eastern and southern boundaries than along the northern and western boundaries, but the latter stays at a prosperous status for two or three more months than the former. Roughly speaking, the boundary cur-

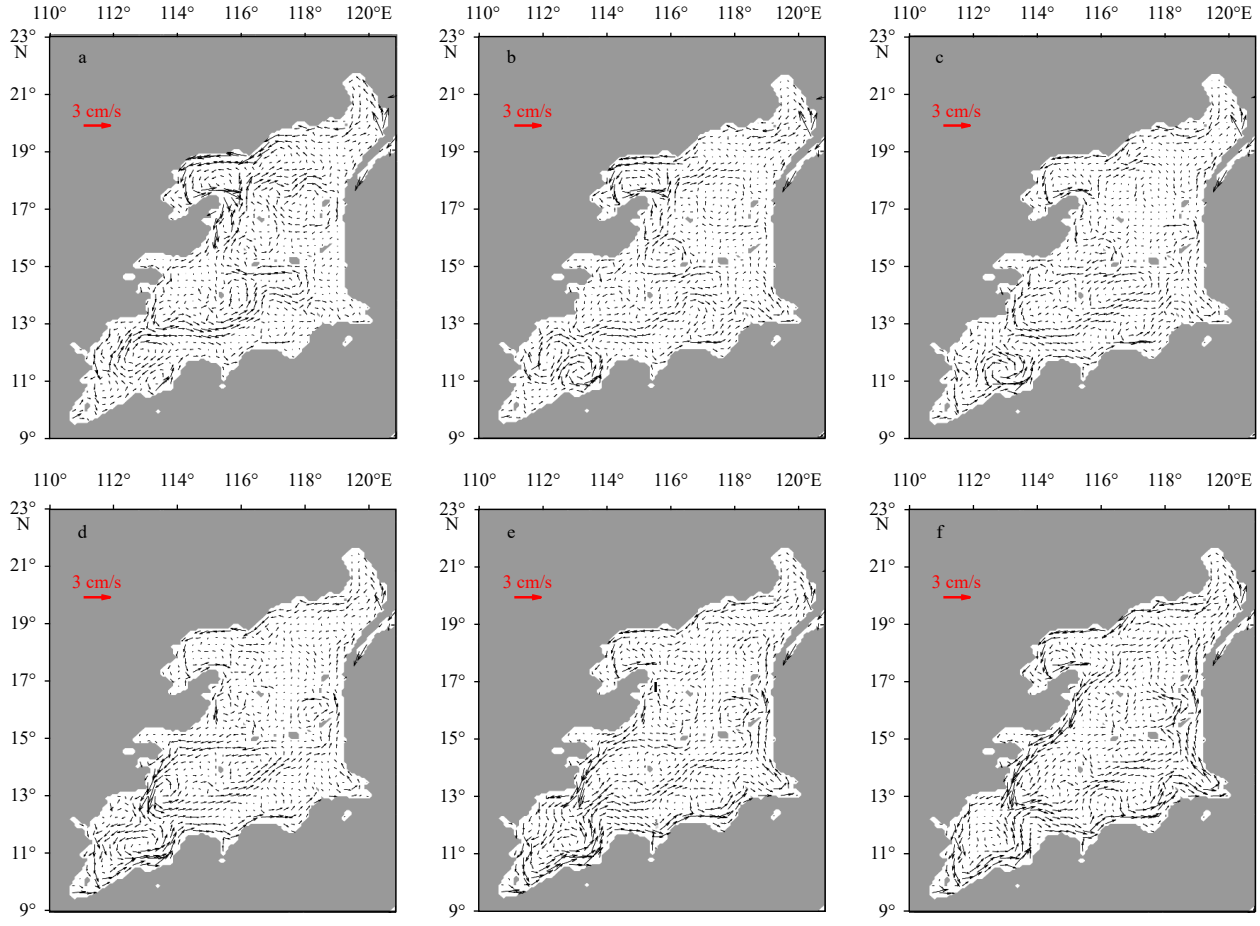

Fig. 3. Monthly mean circulation at 3 000 m in December (a), January (b), February (c), March (d), April (e), and May (f).

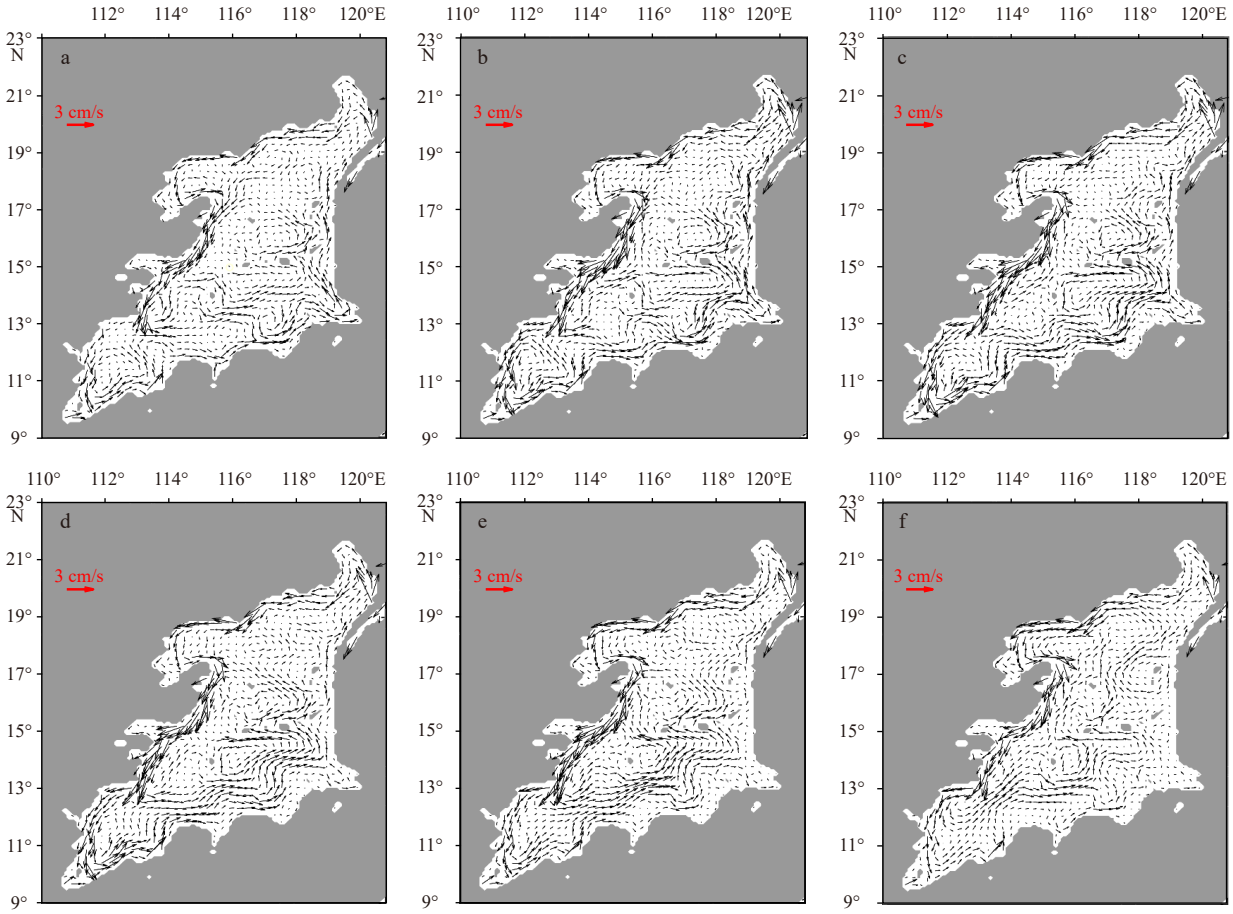

Fig. 4. Monthly mean circulation at 3 000 m in June (a), July (b), August (c), September (d), October (e), and November (f).

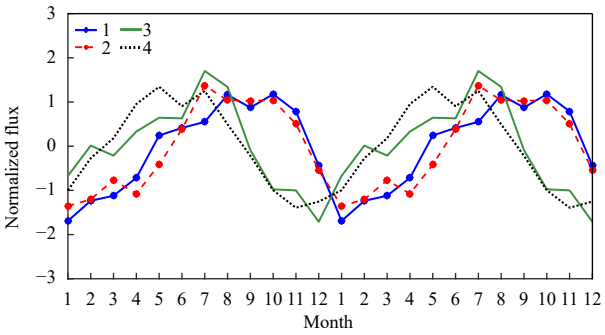

Fig. 5. Annual cycle of normalized fluxes through boundary transects. Transects 1, 2, 3, and 4 indicate the northern, western, southern, and eastern boundaries, respectively.

rents strengthen in the first half year and weaken in the second half, with their weakest fluxes in December or January, and strongest fluxes in July or August. The phase lag of the currents along the western and northern boundaries relative to those along the eastern and southern boundaries needs to be investigated in the further studies.

3.3 *The VEOF modes*

With annual cycle removed, the current velocity fields are decomposed by VEOF analysis for fluctuations in other possible time-scales. The first four VEOF modes account for 63% of the total variance. The periods of major variations above the 95% confidence level are all shorter than one year. The associated spatial patterns reveal that the significant variations are primarily confined in the western and northern boundaries as well as the SW sub-basin. Along the eastern boundary, in the NE and central sub-basins, the variation of the deep circulation is relatively weak, according with the insignificant STDs of velocity components there.

3.3.1 *The first VEOF mode*

The first VEOF mode explains 25.88% of the total variance. The spatial pattern of the first VEOF mode is characterized by a strong DWBC and eddy in the SW sub-basin (Fig. 6a). Power spectrum density of the PC shows significant variations with period of 173 d and 255 d above the 95% confidence level (Figs 6b, c). There is no significant fluctuation with period longer than a year. The most remarkable feature seen from wavelet analysis is that strength of the fluctuation varies year to year. For example, fluctuations with period of 255 d were rather weak between 2002 and 2004, but they reached the greatest amplitude in March 1997 and produced an anomalous southwestward velocity of 8 cm/s in the DWBC and cyclonic eddy in the SW sub-basin (Fig. 6d). The second greatest amplitude occurred in September 2009 when the semi-annual and annual variations co-occurred. The anomalous velocity at the DWBC reached up to 6 cm/s. In these cases, the anomalous southwestward DWBC and cyclonic SW eddy were favorable to the mean circulation pattern and greatly strengthening

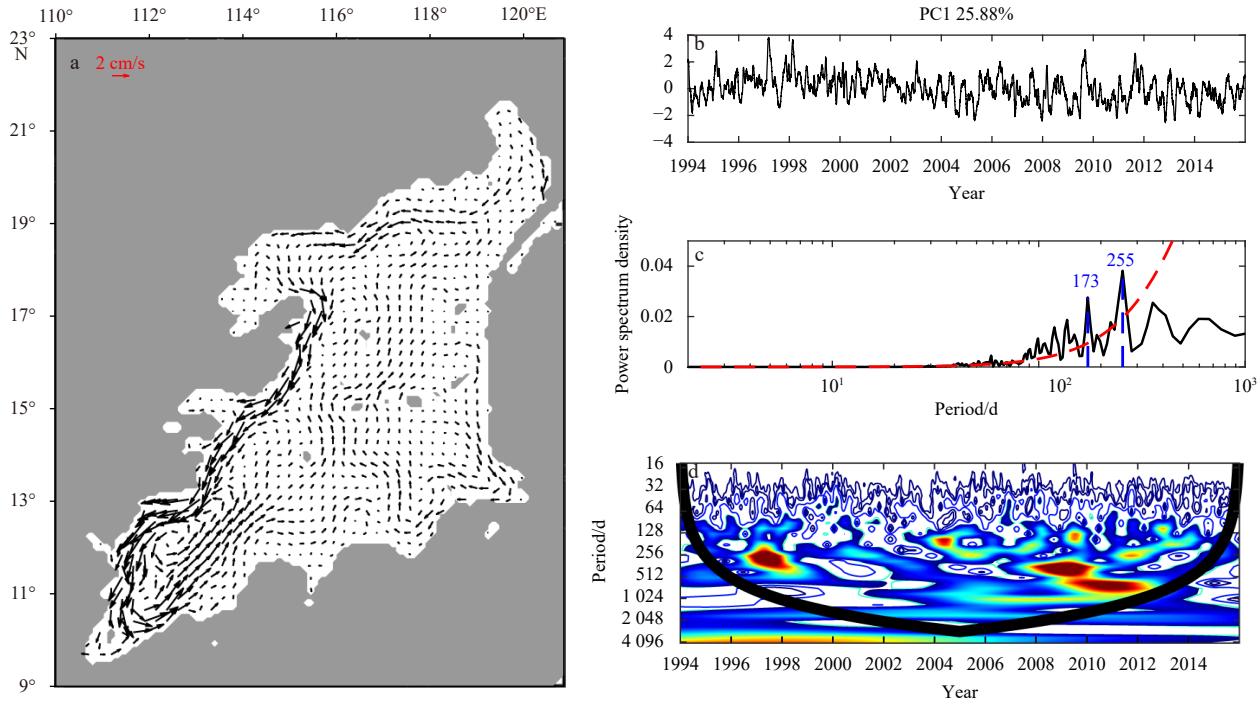

Fig. 6. Spatial structure (a), temporal variation (b), associated power spectrum density (c) and wavelet analysis (d) of the first VEOF mode.

the latter. The fluctuations with period of 173 d are significant most of time except in its weak phase between 1998 and 2004.

3.3.2 *The second VEOF mode*

The second VEOF mode contributes 14.2% of the total variance. Spatial pattern demonstrates a strong eddy in the SW sub-basin and associated basin-scale gyre in the southern SCS. In the northern SCS, a relatively weak gyre is opposite to the southern gyre and extended from the NW sub-basin to the east (Fig. 7a). PC of the second VEOF mode shows intraseasonal fluctuations

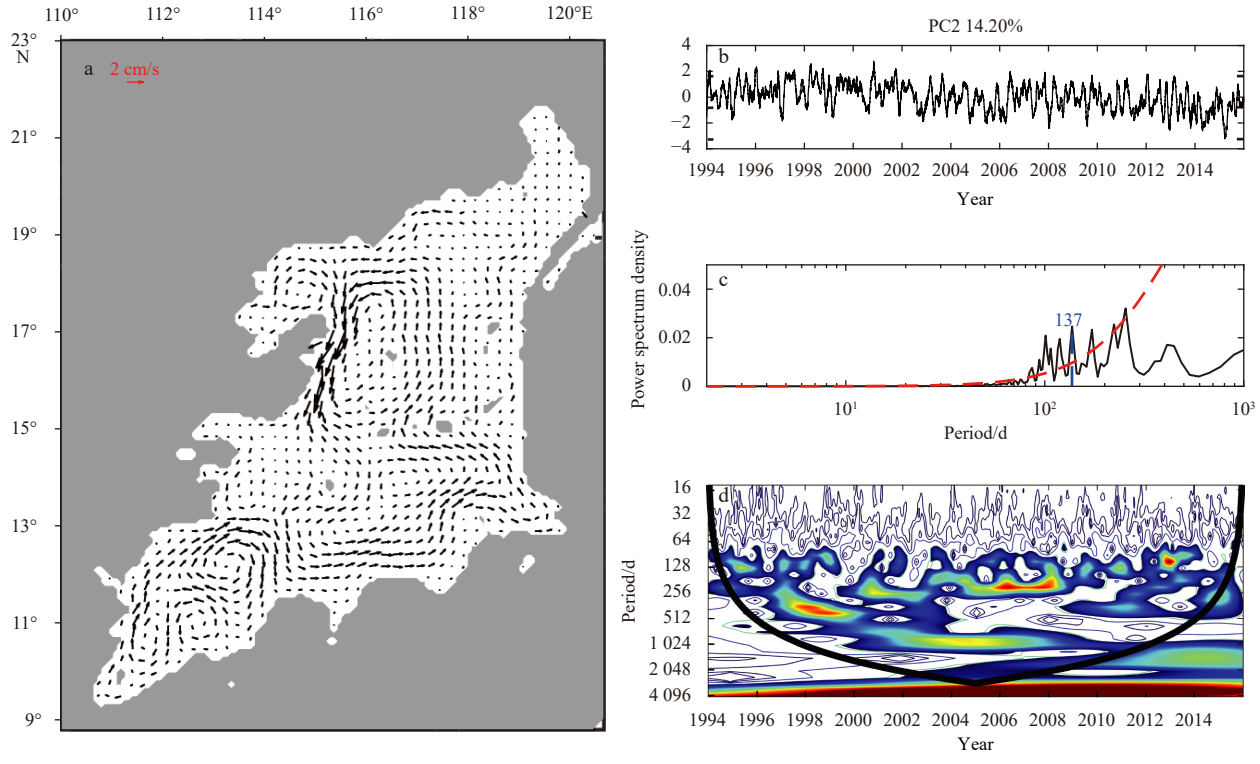

Fig. 7. Spatial structure (a), temporal variation (b), associated power spectrum density (c) and wavelet analysis (d) of the second VEOF mode.

above the 95% confidence level, with dominant fluctuations in 137 d (Figs 7b, c). The greatest amplitude occurred in March 2006, during which the anomalous velocity reached up to 4 cm/s. In the SW sub-basin, the strong anomalous anticyclonic eddy is opposite to the mean pattern and tends to largely weaken the cyclonic eddy. When the PC2 is negative, the anomalous velocities in Fig. 7a are reversed in direction. The negative extreme value of the PC2 reached –3 in March 2015. Multiplying by the velocity scale of 2 cm/s, it can produce an anomalous velocity of –6 cm/s. Under the circumstance, a strong cyclonic eddy with maximum velocity of 6 cm/s would strengthen the eddy in the SW sub-basin greatly. In the meantime, the anomalous anticyclonic gyre in the northern SCS would weaken the mean boundary circulation there. Wavelet analysis shows an interannual discrepancy in intraseasonal fluctuations. The fluctuation with period of 137 d was weak from 1998 to 2000 and from 2001 to 2003, but energetic in the rest years (Fig. 7d).

3.3.3 *The third VEOF mode*

The third VEOF mode contributes 11.5% of the total variance. Spatial pattern mainly contains a strong DWBC from 15°N to 18°N and the associated gyre (Fig. 8a). PC and its power spectrum density show intraseasonal fluctuations above the 95% confidence level, among which the fluctuation with period of 84 d is dominant (Figs 8b, c). The greatest amplitude of PC approached 3.7 in January 1997. This produced an anomalous southwestward velocity of 7.4 cm/s in the DWBC area, greatly enhancing the southwestward boundary circulation. Wavelet analysis indicates the second greatest amplitude of this fluctuation occurring in 2013 (Figs 8b, d). With a PC amplitude of 3, it produces an anomalous southwestward velocity of 6 cm/s, strengthening the DWBC in the time-mean pattern. This fluctuation is supported by observations southeast of the Zhongsha Islands between August 2012 and January 2014 in Zhou et al. (2017). During the observation, the southwestward along-slope velocity demonstrated a fluctuation of 90 d, fairly close to the dominant fluctuation of 84 d derived from the power spectrum analysis based on the HYCOM GOFS3.1 reanalysis. The negative extreme amplitude in late 2009 resulted from a semiannual fluctuation as indicated by wavelet analysis (Fig. 8d). The PC amplitude of –4 produces an anomalous northeastward velocity of 8 cm/s in the DWBC area, largely weakening or even temporarily opposite to the mean DWBC pattern. Wavelet analysis also shows intraseasonal fluctuation with period of 84 d was very weak from 2001 to 2005, whereas a fluctuation with period of 120 d occurred in late 2002 to early 2003.

3.3.4 *The fourth VEOF mode*

The fourth VEOF mode explains 11.4% of the total variance. Spatial pattern is mainly characterized by a dipole eddies in the SW sub-basin (Fig. 9a). The period of the dominant fluctuation is 84 d (Figs 9b, c), nevertheless, the strength differs from year to year (Fig. 9d). The maximum amplitude of PC in February 2006 produced an anomalous velocity of 4 cm/s, forming a strong dipole eddies in the SW sub-basin, that is, a cyclonic eddy in the west and an anticyclonic eddy in the east. This fluctuation also occurred at the beginning of 1998, 2000 and 2013. When the principal component turns negative, the dipole eddies become anticyclonic in the west and cyclonic in the east, which is captured in the January mean climatology. In particular, when the negative extreme amplitude of PC reached –3.7 in the end of 1999, it produced a strong dipole eddies with anomalous velocity of 7.4 cm/s, which is anticyclonic in the west and cyclonic in the east.

3.4 *Trend in the deep SCS circulation*

The trend or long-term change in the deep circulation is difficulty to be observed directly. But it is important to the climate change and thus greatly attracts scientists' attention. For ex-

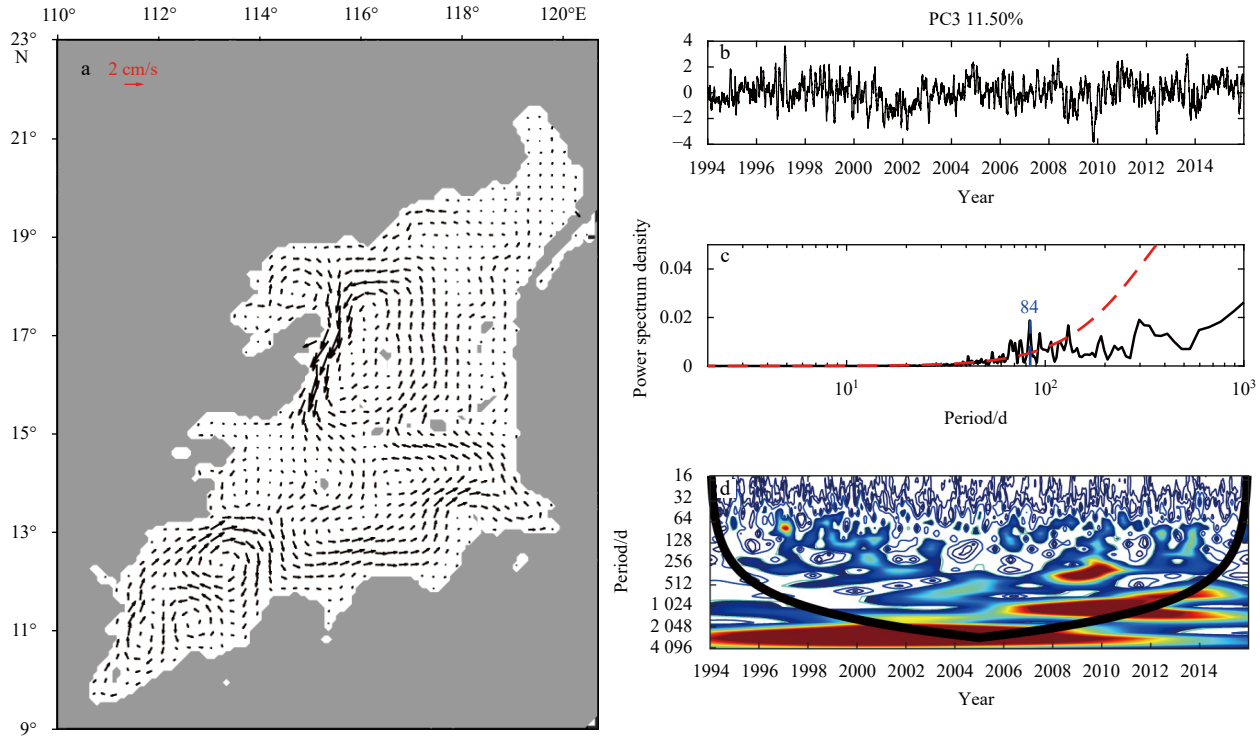

Fig. 8. Spatial structure (a), temporal variation (b), associated power spectrum density (c) and wavelet analysis (d) of the third VEOF mode.

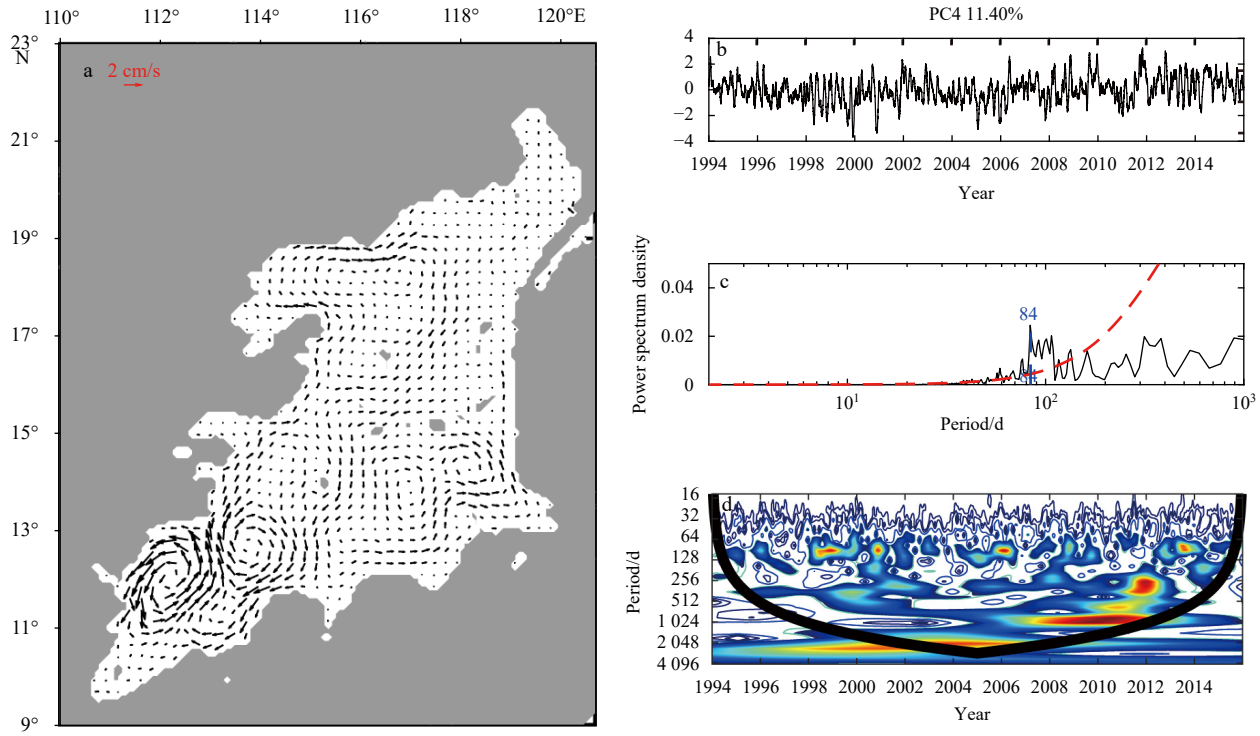

Fig. 9. Spatial structure (a), temporal variation (b), associated power spectrum density (c) and wavelet analysis (d) of the fourth VEOF mode.

ample, based on the Gravity Recovery and Climate Experiment satellite data, Koelling et al. (2020) observed a large-scale anticyclonic circulation anomaly off the North American coast. The difference between the mean geostrophic transport from 2010 to 2017 and mean geostrophic transport from 2002 to 2009 reveals a northward anomaly of $(10.7\times10^6\pm3.3\times10^6)$ m^3/s in the DWBC between 30°–40°N. This anomaly is largely balanced by a southward anomaly of $(13.9\times10^6\pm3.3\times10^6)$ m^3/s west of Mid-Atlantic Ridge. Hitherto, the trend of the deep SCS circulation is not in focus yet. In the present study, we initially derive the linear trend of the velocity field in the deep SCS circulation from the 22-year HYCOM reanalysis data. The velocity trend above the 95% confidence level is depicted in Fig. 10a. The result manifests an anticyclonic circulation anomaly in the deep SCS basin similar to the decadal weakening in the North Atlantic. It includes northeastward currents off the northern slope, northward currents off the western boundary and an anticyclonic eddy in the SW sub-basin. The maximum velocity trend approaches 2 cm/s per decade along the northern slope and in the SW sub-basin. This negative trend tends to weaken the mean cyclonic circulation in the western part of the deep basin. It is noteworthy that the anticyclonic currents in the western and northern boundaries do not lean immediately on but about 50–70 km off the slope. The negative trend is not significant in the eastern and southern boundaries, nor in the western boundary between 14°N and 17°N. The SE sub-basin is an exception, where an anomalous cyclonic eddy there tends to strengthen the mean pattern with a rate of 2 cm/s per decade.

Decadal change is also revealed by the difference between the mean circulation from 2006 to 2015 and mean circulation from 1996 to 2005. It basically repeats the aforementioned linear velocity trend and also fills up missing arrows in the blank areas (Fig. 10b). The decadal change is highly consistent with the linear trend in magnitude and direction of the current velocity, showing itself a good proxy of the linear trend. Initially derived from the HYCOM reanalysis data, the anomalous anticyclonic circulation in the deep SCS is of a potential significance. Confirmation of the decadal trend with observations is to be carried out. Future work should also focus on revealing the dynamics that regulate the mechanism of the decadal weakening. We hope the preliminary work here may offer some beneficial enlightenments to the ongoing study on the long-term change of the deep SCS circulation.

4 Summary

Based on the 22-year HYCOM GOFS3.1 reanalysis product, we investigated the variability of the deep SCS circulation. The results show the current velocity field at 3 000 m is a good proxy of the deep layer circulation. Summary and conclusions are as follows.

(1) Annual variation is a dominant component in the deep SCS circulation. Monthly mean climatology reveals the boundary circulation is of the weakest strength in January, grows in the following months, and peaks between June and September. The currents in the eastern/southern boundary strengthen one to three months earlier than those in the western/northern boundary, and weaken two to three months earlier than the latter as well.

(2) VEOF analysis of the current fields revealed the significant semiannual and intraseasonal fluctuations above the 95% confidence level, but no significant variations with periods over a year. This indicates that the longer time-scale variations in the deep SCS circulation are secondary. Spatial patterns manifest the significant variations are mainly confined in the western boundary area and SW sub-basin. Wavelet analysis indicates strength of the significant semiannual and intraseasonal fluctuations varies year to year.

(3) Based on the HYCOM GOFS3.1 reanalysis data, we initially propose a decadal weakening trend in the deep SCS circulation. The anomalous anticyclonic boundary circulation in the SW

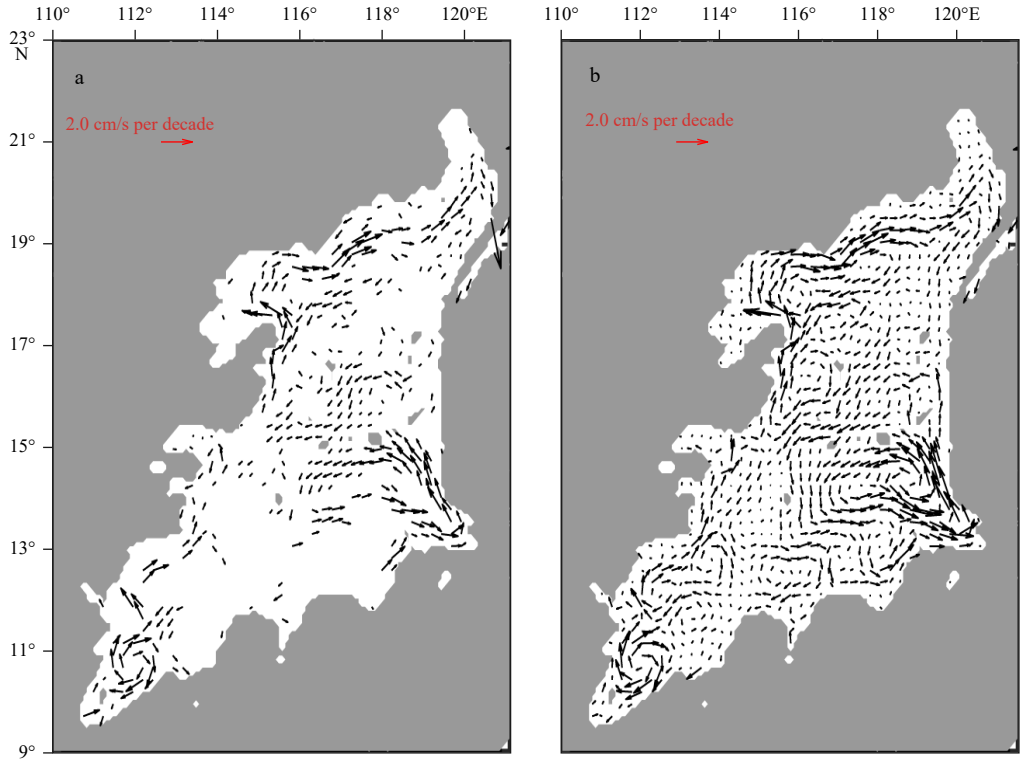

Fig. 10. The linear trend of current velocity (a), and decadal change of deep circulation (b) (2006–2015 mean minus 1996–2005 mean). In a, only the trend above the 95% confidence level is presented.

sub-basin, western and northern boundaries tends to weaken the mean cyclonic circulation pattern with a rate of 2 cm/s per decade. The core of the anomalous anticyclonic boundary circulation does not lean immediately on the continental slope, but about 50–70 km apart from the slope break. In the SE sub-basin, the anomalous cyclonic eddy tends to exceptionally strengthen the mean circulation pattern there. We notice this decadal weakening trend of the DWBC in the SCS is quite similar to the observed decadal weakening in the northwestern Atlantic Deep Basin. This might bring more issues to be addressed in the future.

References

Chao S Y, Shaw P T, Wu S Y. 1996. Deep water ventilation in the South China Sea. Deep-Sea Research Part I: Oceanographic Research Papers, 43(4): 445–466. doi: 10.1016/0967-0637(96)00025-8

Fang Guohong, Chen Haiying, Wei Zexun, et al. 2006. Trends and interannual variability of the South China Sea surface winds, surface height, and surface temperature in the recent decade. Journal of Geophysical Research: Oceans, 111(C11): C11S16, doi: 10.1029/2005JC003276

Gan Jianping, Liu Zhiqiang, Hui C R. 2016a. A three-layer alternating spinning circulation in the South China Sea. Journal of Physical Oceanography, 46(8): 2309–2315. doi: 10.1175/JPO-D-16-0044.1

Gan Jianping, Liu Zhiqiang, Liang Linlin. 2016b. Numerical modeling of intrinsically and extrinsically forced seasonal circulation in the China Seas: A kinematic study. Journal of Geophysical Research: Oceans, 121(7): 4697–4715. doi: 10.1002/2016JC011800

Koelling J, Send U, Lankhorst M. 2020. Decadal strengthening of interior flow of North Atlantic Deep Water observed by GRACE satellites. Journal of Geophysical Research: Oceans, 125(11): e2020JC016217, doi: 10.1029/2020JC016217

Lan Jian, Wang Yu, Cui Fengjuan, et al. 2015. Seasonal variation in the South China Sea deep circulation. Journal of Geophysical Research: Oceans, 120(3): 1682–1690

Lan Jian, Zhang Ningning, Wang Yu. 2013. On the dynamics of the South China Sea deep circulation. Journal of Geophysical Research: Oceans, 118(3): 1206–1210. doi: 10.1002/jgrc.20104

Li Li, Qu Tangdong. 2006. Thermohaline circulation in the deep South China Sea basin inferred from oxygen distributions. Journal of Geophysical Research: Oceans, 111(C5): C05017, doi: 10.1029/2005JC003164

Qu Tangdong, Girton J B, Whitehead J A. 2006. Deepwater overflow through Luzon Strait. Journal of Geophysical Research: Oceans, 111(C1): C01002, doi: 10.1029/2005JC003139

Shao Lei, Li Xuejie, Geng Jianhua, et al. 2007. Deep water bottom current deposition in the northern South China Sea. Science in China Series D: Earth Sciences, 50(7): 1060–1066

Shu Yeqiang, Xue Huijie, Wang Dongxiao, et al. 2014. Meridional overturning circulation in the South China Sea envisioned from the high-resolution global reanalysis data GLBa0.08. Journal of Geophysical Research: Oceans, 119(5): 3012–3028. doi: 10.1002/2013JC009583

Tian Jiwei, Yang Qingxuan, Zhao Wei. 2009. Enhanced diapycnal mixing in the South China Sea. Journal of Physical Oceanography, 39(12): 3191–3203

Wang J. 1986. Observation of abyssal flows in the Northern South China Sea. Acta Oceanographica Taiwanica, 16: 36– 45

Wang Yonggang, Fang Guohong, Wei Zexun, et al. 2006. Interannual variation of the South China Sea circulation and its relation to El Niño, as seen from a variable grid global ocean model. Journal of Geophysical Research: Oceans, 111(C11): C11S14

Wang Guihua, Xie Shangping, Qu Tangdong, et al. 2011. Deep South China Sea circulation. Geophysical Research Letters, 38(5): L05601, doi: 10.1029/2010GL046626

Wang Bin, Zhao Wei. 2013. The influence of horizontal resolution on the numerical simulation of deep water circulation in Luzon Strait. Periodical of Ocean University of China, 43(4): 1–8

Wu C R, Shaw P T, Chao S Y. 1998. Seasonal and interannual variations in the velocity field of the South China Sea. Journal of Oceanography, 54(4): 361–372

Wyrtki K. 1961. Scientific results of marine investigations of the South China Sea and the Gulf of Thailand 1959– 1961: Physical oceanography of the Southeast Asian waters. La Jolla, CA, USA: Scripps Institute of Oceanography

Xiao Jingen, Xie Qiang, Liu Changjian, et al. 2013. A diagnostic model of the South China Sea bottom circulation in consideration of tidal mixing, eddy-induced mixing and topography. Haiyang Xuebao (in Chinese), 35(5): 1–13. doi: 10.3969/j.issn.0253-4193.2013.05.001

Xie Qiang, Xiao Jingen, Wang Dongxiao, et al. 2013. Analysis of deep-layer and bottom circulations in the South China Sea based on eight quasi-global ocean model outputs. Chinese Science Bulletin, 58(23): 4000–4011. doi: 10.1007/s11434-013-5791-5

Xu Fanghua, Oey L Y. 2014. State analysis using the Local Ensemble Transform Kalman Filter (LETKF) and the three-layer circulation structure of the Luzon Strait and the South China Sea. Ocean Dynamics, 64(6): 905–923. doi: 10.1007/s10236-014-0720-y

Xu Tengfei, Wei Zexun, Susanto R D, et al. 2021. Observed water exchange between the South China Sea and Java Sea through Karimata Strait. Journal of Geophysical Research: Oceans, 126(2): e2020JC016608, doi: 10.1029/2020JC016608

Yuan Dongliang. 2002. A numerical study of the South China Sea deep circulation and its relation to the Luzon Strait transport. Acta Oceanologica Sinica, 21(2): 187–202

Zhang Zhiwei, Zhao Wei, Tian Jiwei, et al. 2015. Spatial structure and temporal variability of the zonal flow in the Luzon Strait. Journal of Geophysical Research: Oceans, 120(2): 759–776. doi: 10.1002/2014JC010308

Zhao Wei, Zhou Chun, Tian Jiwei, et al. 2014. Deep water circulation in the Luzon Strait. Journal of Geophysical Research: Oceans, 119(2): 790–804. doi: 10.1002/2013JC009587

Zheng Hua, Zhang Chuanzheng, Zhao Ruixiang, et al. 2021. Structure and variability of abyssal current in northern South China Sea based on CPIES observations. Journal of Geophysical Research: Oceans, 126(4): e2020JC016780, doi: 10.1029/2020JC016780

Zhou Chun, Zhao Wei, Tian Jiwei, et al. 2014. Variability of the deep-water overflow in the Luzon Strait. Journal of Physical Oceanography, 44(11): 2972–2986

Zhou Chun, Zhao Wei, Tian Jiwei, et al. 2017. Deep western boundary current in the South China Sea. Scientific Reports, 7(1): 9303, doi: 10.1038/s41598-017-09436-2

Zhou Chun, Zhao Wei, Tian Jiwei, et al. 2018. Observations of deep current at the western boundary of the Northern Philippine Basin. Scientific Reports, 8(1): 14334, doi: 10.1038/s41598-018-32541-9

Zhu Yaohua, Sun Junchuan, Wang Yonggang, et al. 2017a. Effect of potential vorticity flux on the circulation in the South China Sea. Journal of Geophysical Research: Oceans, 122(8): 6454–6469. doi: 10.1002/2016JC012375

Zhu Yaohua, Sun Junchuan, Wang Yonggang, et al. 2019. Overview of the multi-layer circulation in the South China Sea. Progress in Oceanography, 175: 171–182. doi: 10.1016/j.pocean.2019.04.001

Zhu Yaohua, Sun Junchuan, Wei Zexun, et al. 2017b. A fresh look at the deepwater overflow in the Luzon Strait. Acta Oceanologica Sinica, 36(5): 1–8. doi: 10.1007/s13131-017-1057-4

Appendix:

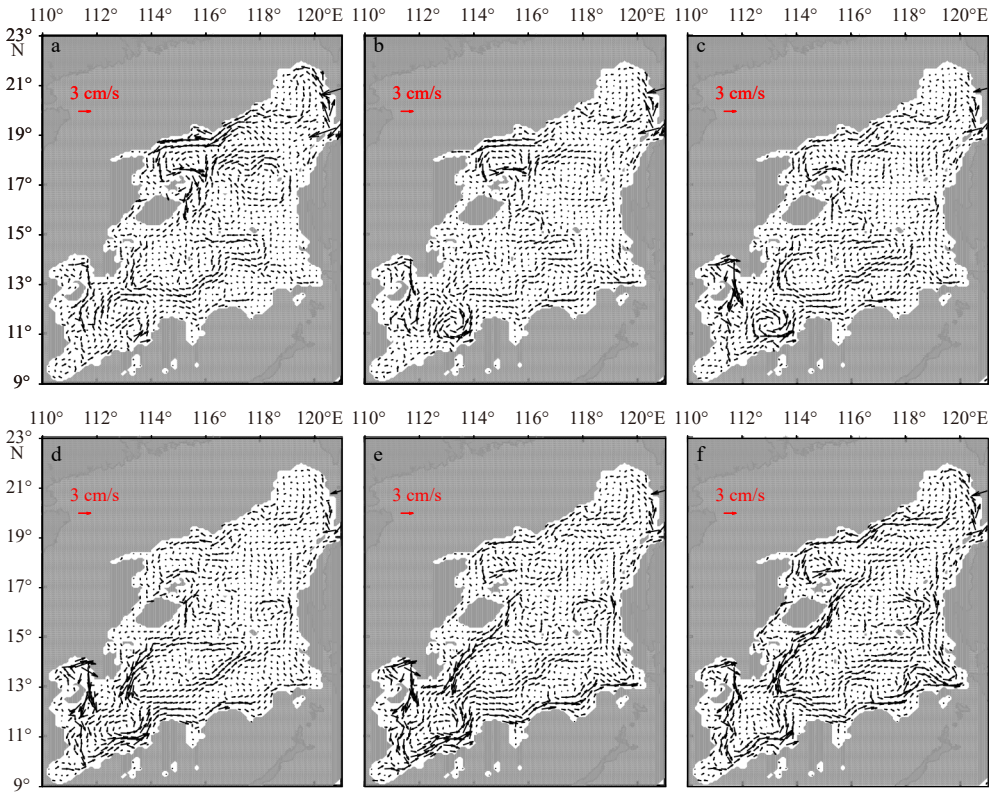

Fig. A1. Monthly mean circulation averaged between 2 500 m and 4 000 m in December (a), January (b), February (c), March (d), April (e), and May (f).

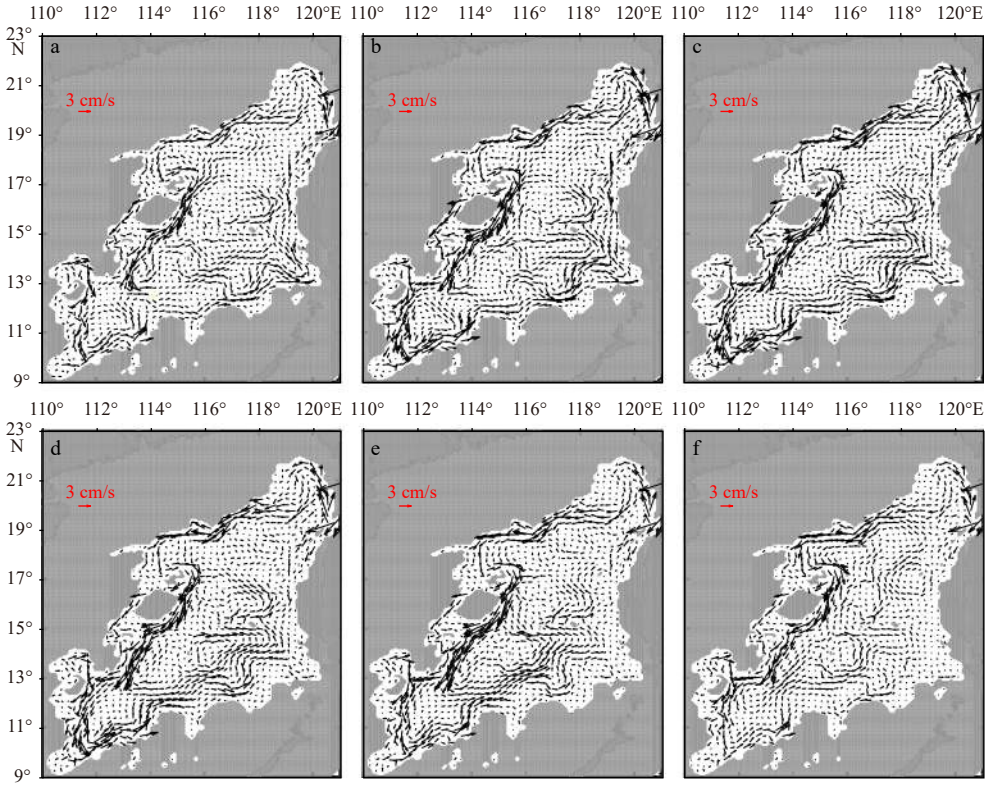

Fig. A2. Monthly mean circulation averaged between 2 500 m and 4 000 m in June (a), July (b), August (c), September (d), October (e), and November (f).